Designing Decentralized Load-Frequency Controllers

AN OPTIMIZATION APPROACH FOR SYNCHRONOUS GENERATORS IN ISLANDED GRIDS

©ISTOCKPHOTO.COM/SCYTHER5

By S. Mohsen Azizi and S. Ali Khajehoddin

Digital Object Identifier 10.1109/MIAS.2017.2740472
Date of publication: 3 January 2018

IN THIS ARTICLE, AN OPTIMAL DECENTRALIZED CONTROLLER IS DESIGNED FOR the load-frequency control (LFC) of a multiarea islanded grid with multiple synchronous generation systems. The decentralized controller includes various proportional-integral (PI) controllers that are simultaneously designed and optimized by using a classical descent-direction quasi-Newton (QN)-based technique. Optimal decentralized PI controllers account for the dynamic coupling amid the areas of the islanded grid with no communication links among them required and, hence, improve the frequency control performance. Simulation results confirm the effectiveness of the proposed decentralized PI control approach. The suggested PI controllers have a similar performance to decentralized eighth-order, linear-quadratic-Gaussian (LQG) integral controllers, which

are designed in the decentralized servomechanism framework, whereas the proposed decentralized PI controllers have considerably lower-order structures.

LFC Overview

In an islanded grid in which the synchronous generators are relatively large (compared to the other distributed generation systems), the synchronous generators mainly control the voltage and frequency. The LFC and automatic-voltage-regulator (AVR) systems exist in each synchronous generator to compensate for the impact of load changes in the frequency and voltage of the grid. The magnitude of these changes are associated with those of the real (ΔP_G) and reactive (ΔQ_G) powers, respectively. However, the dynamics of the two control loops are considered as decoupled because the time constant of the prime mover (in LFC) is considerably greater than that of the excitation system (in an AVR). To this end, this article focuses on the LFC loop only, which is important for the performance of the islanded grid when disconnecting from or connecting to the main grid or when the power generated by the other distributed generation systems drastically changes. Therefore, an optimal controller is needed to improve the steady-state and transient responses of the grid, which is studied in detail in this article. Designing a controller whose performance is robust to the parameter changes of the system is investigated by the authors in [1].

The LFC problem has been tackled in the literature by different techniques. In [2], the performance of the LFC loop is improved by using a decentralized sliding mode control with a PI switching surface. In [3], a decentralized fuzzy-logic-based scheme is used to solve the LFC problem in the presence of high-penetration wind power, and the particle-swarm optimization technique is used to calculate the parameters of membership functions. In [4], a direct–indirect adaptive fuzzy-control technique is used for the LFC control problem of power systems, in which the unknown parameters of interconnected power areas are estimated using adaptive control laws, and the estimation errors and external disturbance effects are minimized using an H_∞ tracking criteria. In [5], a fuzzy PI controller scheme in which PI gains are adaptively adjusted by using fuzzy rules based on area control errors (ACEs), and a genetic algorithm and particle-swarm optimization technique is used to minimize the errors.

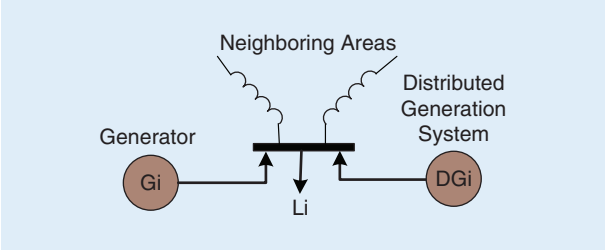

FIGURE 1. An islanded grid area. Gi: generator; DGi: distributed generator; Li: load of the area *i*.

The LFC problem is approached in [6] using the PI-differential controller, which is optimized by the Lozi map-based chaotic algorithm. In [7], a differential game-theory approach is applied for the cooperative control of load frequency in multiple areas by using the conflict resolution capability of the algorithm. A multiagent reinforcement learning approach is employed in [8] for the LFC problem in power systems, where the ACEs are estimated to tune the controller parameters and improve the control performance. The authors in [9] used an internal model control scheme with two degrees of freedom, in which a reduced-order model of the system is considered for the design of a reduced-order LFC system for disturbance rejection. In [10], a decentralized optimal control scheme is used to solve the LFC problem in distributed power systems by implementing neighborhood area communication, which mitigates the inconsistencies in local estimates.

In most LFC techniques in the literature, either the control method is nonlinear (or linear time varying) or the controller performance depends on communication links throughout the grid. In this article, the PI controller structure is selected, which makes the design, stability analysis, and implementation of the controller straightforward due to its simple linear time-invariant structure [11]. Moreover, a classical descent-direction QN-based optimization technique is applied to simultaneously optimize the performances of all local PI controllers. The augmented configuration of the simultaneously optimized local PI controllers, i.e., the optimal decentralized PI controller, does not require any communication among the local controllers of the islanded grid.

LFC System

The LFC system measures the frequency (ΔFreq) and tie-line power (ΔP_{tie}) errors and sends the control command for changing the valve position error (ΔP_v) to the prime mover [12], [13]. The notation Δ, which will be used throughout this article, stands for the deviation (error) of a variable from its desired value (reference). Figures 1 and 2 demonstrate the block diagrams of an islanded grid and a generator LFC loop, respectively.

The generators are coupled through the tie lines indicated in Figure 3. In Figure 2, the term $r_i \triangleq \Delta P_{d,i} + \Delta P_{L,i}$ represents the impacts of the local distributed generation systems ($\Delta P_{d,i}$) and the local loads ($\Delta P_{L,i}$). For each area i in Figure 2, the dynamic parameters are specified in Table 1. The turbine, generator, and governor transfer functions are represented by

$$T_{\text{turb},i} = \frac{1}{\tau_{cb,i}s + 1},$$

$$T_{\text{gen},i} = \frac{1}{M_i s + D_i},$$

$$T_{\text{gov},i} = \frac{1}{\tau_{g,i}s + 1},$$

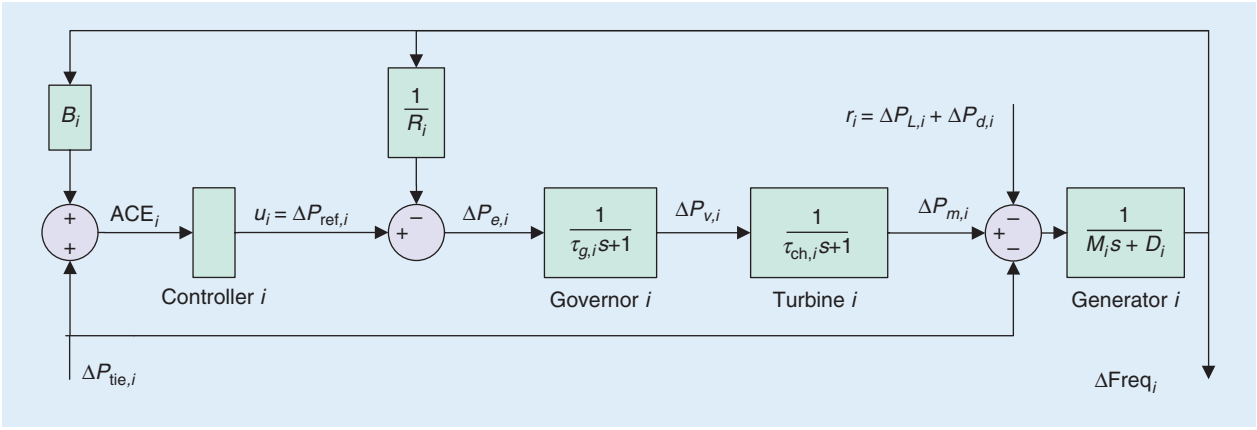

FIGURE 2. A block diagram of a generator.

respectively, based on which associated area transfer functions are determined

$$
\begin{aligned}
T_{\Delta\text{Freq}_i/r_i} &= \frac{-T_{\text{gen},i}}{1 + T_{\text{gen},i}T_{\text{turb},i}T_{\text{gov},i}/R_i},\\
T_{\Delta\text{Freq}_i/\Delta P_{\text{ref},i}} &= \frac{T_{\text{gen},i}T_{\text{turb},i}T_{\text{gov},i}}{1 + T_{\text{gen},i}T_{\text{turb},i}T_{\text{gov},i}/R_i},\\
T_{\Delta\text{Freq}_i/\Delta P_{\text{tie},i}} &= \frac{T_{\text{gen},i}}{1 + T_{\text{gen},i}T_{\text{turb},i}T_{\text{gov},i}/R_i},\\
T_{\text{ACE}_i/r_i} &= B_i T_{\Delta F_i/\Delta P_{\text{tie},i}},\\
T_{\text{ACE}_i/\Delta P_{\text{ref},i}} &= B_i T_{\Delta F_i/U_i},\\
T_{\text{ACE}_i/\Delta P_{\text{tie},i}} &= 1 + B_i T_{\Delta F_i/\Delta P_{\text{tie},i}},
\end{aligned}
\tag{1}
$$

where T_{Y_i/U_i} represents the transfer function from input $U_i \in \{r_i, \Delta P_{\text{ref},i}, \Delta P_{\text{tie},i}\}$ to output $Y_i \in \{\Delta\text{Freq}_i, \text{ACE}_i\}$.

In Figure 2, the governor block stabilizes the grid operation by allowing the frequency to drop when the load increases. The load power changes linearly as a function of the frequency according to the droop equation

$$
P_{e,i} = \Delta P_{\text{ref},i} - \frac{1}{R_i}\text{Freq}_i. \tag{2}
$$

As indicated in Figure 2, the ACE is given as input to the controller i. The frequency-response characteristic (bias factor) defined by $B_i = (1/R_i) + D_i$ is used to calculate the ACE defined by $\text{ACE}_i = \Delta P_{\text{tie},i} + B_i \Delta\text{Freq}_i$, which consists of a linear combination of the frequency error (with the coefficient 1) and the tie-line error (with the coefficient B_i). The objective of the LFC is to regulate the frequency and tie-line errors by forcing the ACE to converge to zero.

The block diagram of the tie-line interconnection block in Figure 2 is depicted in Figure 3. In this figure, T_{ij}, which is also included in Table 1, represents the tie-line synchronizing torque coefficient between areas i and j of the islanded grid. As indicated in this figure, the tie-line power error is the integral of the frequency difference between the two areas of the grid. Therefore, $\Delta P_{\text{tie},i}$ is calculated by

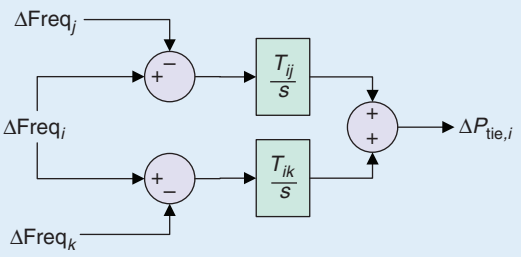

FIGURE 3. A block diagram of tie-line interconnections.

Table 1. The dynamic parameters of each area

ΔFreq_i	Frequency error (Hz)
$\Delta P_{L,i}$	Load power error (p.u.)
$\Delta P_{\text{tie},i}$	Tie-line power error (p.u.)
$\Delta P_{m,i}$	Mechanical power error (p.u.)
$\Delta P_{v,i}$	Valve position error (p.u.)
$\Delta P_{e,i}$	$\Delta P_{\text{ref},i} - (\Delta\text{Freq}_i/R_i)$ (p.u.)
$\Delta P_{\text{ref},i}$	Reference set power error (p.u.)
$\Delta P_{d,i}$	Distributed generation system power error (p.u.)
ACE_i	ACE (p.u.)
M_i	$2H$ (H: inertia constant) (p.u./s)
D_i	Load-damping constant (p.u./Hz)
$\tau_{ch,i}$	Turbine time constant (s)
$\tau_{g,i}$	Governor time constant (s)
R_i	Frequency droop coefficient or regulator (Hz/p.u.)
B_i	Bias factor, or frequency response characteristic (p.u./Hz)
T_{ij}	Tie-line synchronizing torque coefficient between areas i and j (p.u./rad)

p.u.: per unit.

$$\Delta P_{\text{tie},i} = \sum_{j \neq i} \frac{T_{ij}}{s} (\Delta\text{Freq}_i - \Delta\text{Freq}_j).$$

Augmenting all of the area transfer functions in (1) results in an overall grid transfer function $T_A(s)$ as

$$\begin{bmatrix} \text{ACE} \\ \Delta\text{Freq} \end{bmatrix} = T_A(s) \begin{bmatrix} \Delta P_{\text{ref}} \\ r \\ \Delta P_{\text{tie}} \end{bmatrix},$$
$$T_A(s) = \begin{bmatrix} T_{\text{ACE}/\Delta P_{\text{ref}}} & T_{\text{ACE}/r} & T_{\text{ACE}/\Delta P_{\text{tie}}} \\ T_{\Delta\text{Freq}/\Delta P_{\text{ref}}} & T_{\Delta\text{Freq}/r} & T_{\Delta\text{Freq}/\Delta P_{\text{tie}}} \end{bmatrix},$$

where, for the case of three areas ($i = 1, 2, 3$),

$$\begin{aligned} \text{ACE} &= [\text{ACE}_i]^T_{i=1,2,3}, \\ \Delta\text{Freq} &= [\Delta\text{Freq}_i]^T_{i=1,2,3}, \\ \Delta P_{\text{ref}} &= [\Delta P_{\text{ref},i}]^T_{i=1,2,3}, \\ r &= [r_i]^T_{i=1,2,3}, \\ \Delta P_{\text{tie}} &= [\Delta P_{\text{tie},i}]^T_{i=1,2,3}, \end{aligned}$$

and $T_{Y/U} = \text{diag}(T_{Y_i/U_i})_{i=1,2,3}$ represents the diagonal transfer function matrix from inputs $U = [U_i]^T_{i=1,2,3} \in \{r, \Delta P_{\text{ref}}, \Delta P_{\text{tie}}\}$ to outputs $Y = [Y_i]^T_{i=1,2,3} \in \{\Delta\text{Freq}, \text{ACE}\}$. As indicated in Figure 3, for the case of three areas ($i = 1, 2, 3$), the interconnection transfer function $T_I(s)$ is represented by

$$\Delta P_{\text{tie}} = T_I(s)\Delta\text{Freq},$$
$$T_I(s) = \begin{bmatrix} \frac{T_{12}+T_{13}}{s} & \frac{-T_{12}}{s} & \frac{-T_{13}}{s} \\ \frac{-T_{21}}{s} & \frac{T_{21}+T_{23}}{s} & \frac{-T_{23}}{s} \\ \frac{-T_{31}}{s} & \frac{-T_{32}}{s} & \frac{T_{31}+T_{32}}{s} \end{bmatrix}.$$

The lower linear fractional transformation of the grid transfer function $T_A(s)$ and the interconnection transfer function $T_I(s)$ is represented by $\mathcal{F}_L(T_A(s), T_I(s))$, which yields the following input–output dynamic equation:

$$\text{ACE} = \mathcal{F}_L(T_A(s), T_I(s)) \begin{bmatrix} \Delta P_{\text{ref}} \\ r \end{bmatrix}. \tag{3}$$

The transfer function $\mathcal{F}_L(T_A(s), T_I(s))$ is used in the next section to design a decentralized PI controller.

Decentralized PI Controller Formulation

In this section, a decentralized PI controller is formulated for the dynamic equation in (3). The decentralized controller takes the required measurements to calculate ACE and, based on it, generates the control command ΔP_{ref} such that ACE will converge to zero and the control performance will be robust to the disturbance r. For the controller to be decentralized, its structure should be diagonal as per the following:

$$\begin{bmatrix} K_{P,1} + \frac{K_{I,1}}{s} & 0 & 0 \\ 0 & K_{P,2} + \frac{K_{I,2}}{s} & 0 \\ 0 & 0 & K_{P,3} + \frac{K_{I,3}}{s} \end{bmatrix} =$$
$$\underbrace{\begin{bmatrix} K_{P,1} & 0 & 0 \\ K_{I,1} & 0 & 0 \\ 0 & K_{P,2} & 0 \\ 0 & K_{I,2} & 0 \\ 0 & 0 & K_{P,3} \\ 0 & 0 & K_{I,3} \end{bmatrix}^T}_{K} \times \underbrace{\begin{bmatrix} 1 & 0 & 0 \\ \frac{1}{s} & 0 & 0 \\ 0 & 1 & 0 \\ 0 & \frac{1}{s} & 0 \\ 0 & 0 & 1 \\ 0 & 0 & \frac{1}{s} \end{bmatrix}}_{T_C(s)} = KT_C(s), \tag{4}$$

where both the static feedback gain matrix K and the dynamic matrix $T_C(s)$ have block-diagonal structures. Therefore, the controller dynamic equation is represented by $KT_C(s)$, which generates the control command ΔP_{ref} as a function of ACE as

$$\Delta P_{\text{ref}} = KT_C(s)\text{ACE}. \tag{5}$$

In the rest of this article, for notational simplicity and to transform the system into the standard state-space model, the new variables $y \triangleq T_C(s)\text{ACE}$ and $u \triangleq \Delta P_{\text{ref}}$ are defined. The notations r [in (3)] and u are in line with the variables r_i and u_i in Figure 2 ($r = [r_1\ r_2\ r_3]^T$ and $u = [u_1\ u_2\ u_3]^T$ for the three areas $i = 1, 2, 3$). Using these notations, the system in (3) and the dynamic controller in (5) are simplified and transformed to

$$y = T_C(s)\mathcal{F}_L(T_A(s), T_I(s)) \begin{bmatrix} u \\ r \end{bmatrix}, \tag{6}$$
$$u = Ky. \tag{7}$$

The linear system transfer function in (6) can be transformed into the following equivalent state-space model by using the command tf2ss in MATLAB:

$$\begin{aligned} \dot{x} &= Ax + Bu + Er, \\ y &= Cx + Fr, \\ z &= Mx, \end{aligned} \tag{8}$$

where x, u, r, y, and z represent the state, input, disturbance, measurement output, and performance output vectors, respectively. In this article, for the transfer function (6), we have $z = y$ ($M = C$ and $F = 0$). However, (8) is kept in its general form with $z \neq y$ ($M \neq C$ and $F \neq 0$) to develop an optimization algorithm for the more generic form of the problem in (8).

In the next section, the feedback gain matrix K in (7), for which the decentralized structure is indicated in (4), is calculated and optimized for the state-space model in (8)

such that the performance output z will converge to zero, whereas the control performance will be robust to the disturbance r.

Performance Optimization of the Decentralized PI Controller

In this section, an optimization technique will be used to design the feedback gain matrix K in (7) for the state-space model in (8). The feedback gain matrix K will be optimized such that the performance output z will converge to zero, and the control performance will be robust to the disturbance r, while K will preserve its decentralized structure indicated in (4).

Using the feedback gain matrix K in (7) for the state-space model in (8), the closed-loop system is transformed to

$$\begin{aligned} \dot{x} &= \underbrace{(A+BKC)}_{A_c}x + \underbrace{(E+BKF)}_{B_c}r = A_c x + B_c r,\\ y &= Cx + Fr,\\ z &= Mx. \end{aligned} \tag{9}$$

Taking $r = r_0$ and denoting the steady-state and transient values of a variable by "—" and "~", respectively, the steady-state equations [associated with the closed-loop system in (9) and the feedback gain matrix in (7)] are given by

$$\begin{aligned} \dot{\bar{x}} &= 0 = A_c\bar{x} + B_c r_0 \\ \bar{y} &= C\bar{x} + Fr_0 \\ \bar{z} &= M\bar{x} \\ \bar{u} &= K\bar{x} \end{aligned} \Rightarrow \begin{aligned} \bar{x} &= -A_c^{-1}B_c r_0,\\ \bar{y} &= (-CA_c^{-1}B_c + F)r_0,\\ \bar{z} &= -MA_c^{-1}B_c r_0,\\ \bar{u} &= -KA_c^{-1}B_c r_0, \end{aligned} \tag{10}$$

and the associated transient equations are given by

$$\dot{\tilde{x}} = A_c\tilde{x},\ \ \tilde{y} = C\tilde{x},\ \ \tilde{z} = M\tilde{x},\ \ \tilde{u} = KC\tilde{x}. \tag{11}$$

Based on the steady-state and transient equations (10) and (11), the cost (objective) function of the optimal controller will be formulated and solved.

Cost Function and Optimization Problem Formulation

In this section, the following problem of minimizing the cost function J is considered and solved:

$$\begin{aligned} &\text{Minimize } J = \int_0^\infty (t^k\tilde{z}^T Q\tilde{z} + \tilde{u}^T R\tilde{u})\,dt + \tilde{z}^T V\tilde{z} + \sum_i\sum_j g_{ij}k_{ij}^2,\\ &\text{Subject to } \tilde{u} = K\tilde{y}, \end{aligned} \tag{12}$$

where $Q > 0$, $R > 0$, $V \geq 0$, and $g_{ij} \geq 0$ are constant coefficients with a large magnitude to force a penalty on the 12 zero elements k_{ij} (e.g., k_{13} and k_{34}) of the feedback gain matrix K in (4) and (5) (k_{ij} is the ith-row, jth-column element of the feedback gain matrix K). Out of the four terms in the cost function J in (12), the first three terms will minimize output energy, input energy, and disturbance impact, and the last term will enforce the decentralized, respectively, structure of the feedback gain matrix K in (4) and (5).

For the optimization problem (12) to converge to a locally minimum point, the following five conditions need to be satisfied [14]:

- System matrix A is output stabilizable, which means there exists a matrix K that makes $A + BKC$ Hurwitz.
- System matrix C has full rank.
- Matrices Q and R in (12) are semipositive and positive definite, respectively, i.e., $Q \geq 0$ and $R > 0$.
- The pair $(Q^{1/2}M, A)$ is detectable, where $Q^{1/2}$ is the square root of Q such that $Q = Q^{1/2}Q^{1/2}$.
- The positive integer k is chosen such that the pair $(k!P_{k-1} + C^T K^T RKC, A)$ is detectable, where P_{k-1} is as presented in (14).

The integral term in the minimization problem (12) can be replaced by an equivalent algebraic term subject to several algebraic Riccati constraints as

$$J = \text{trace}(P_k X) + \tilde{z}^T V\tilde{z} + \sum_i\sum_j g_{ij}k_{ij}^2, \tag{13}$$

$$\begin{aligned} \text{Subject to } f_0 &\triangleq A_c^T P_0 + P_0 A_c + M^T QM = 0,\\ f_1 &\triangleq A_c^T P_1 + P_1 A_c + P_0 = 0,\\ &\vdots\\ f_{k-1} &\triangleq A_c^T P_{k-1} + P_{k-1}A_c + P_{k-2} = 0,\\ f_k &\triangleq A_c^T P_k + P_k A_c + k!P_{k-1} + C^T K^T RKC = 0, \end{aligned} \tag{14}$$

where X is defined by using $\bar{x}$ in (10) as

$$X = \bar{x}\bar{x}^T = A_c^{-1}B_c r_0 r_0^T B_c^T A_c^{-T}.$$

To minimize the cost function J in (13) with respect to K, the Lagrangian L is defined as

$$\begin{aligned} L = {} & \text{trace}(P_k X) + \tilde{z}^T V\tilde{z} + \sum_i\sum_j g_{ij}k_{ij}^2,\\ & + \text{trace}(f_0\Lambda_0) + \cdots + \text{trace}(f_k\Lambda_k), \end{aligned} \tag{15}$$

where $\Lambda_0, \ldots, \Lambda_k$ are the Lagrange multipliers for the constraints $f_0, \ldots, f_k$ in (14).

Taking the partial derivatives of L with respect to the Lagrange multipliers $\Lambda_0, \ldots, \Lambda_k$ results in the same set of equations as in (14). Taking the partial derivative of L with respect to K^T results in

$$\begin{aligned} \frac{1}{2}\frac{\partial L}{\partial K^T} = {} & RKC\Lambda_k C^T + B^T(P_0\Lambda_0 + \cdots + P_k\Lambda_k)C^T\\ & - B^T A_c^{-T}(P_k + M^T VM)\bar{x}\bar{y}^T + g * K = 0, \end{aligned} \tag{16}$$

where $g * K$ denotes the elementwise product, and the steady-state values $\bar{x}$ and $\bar{y}$ are defined in (10). Taking the partial derivatives of L with respect to $P_0, \ldots, P_k$ results in the following algebraic Riccati equations:

$$\frac{\partial L}{\partial P_k} = A_c\Lambda_k + \Lambda_k A_c^T + X = 0,$$
$$\frac{\partial L}{\partial P_{k-1}} = A_c\Lambda_{k-1} + \Lambda_{k-1}A_c^T + k!\Lambda_k = 0,$$
$$\frac{\partial L}{\partial P_{k-2}} = A_c\Lambda_{k-2} + \Lambda_{k-2}A_c^T + \Lambda_{k-1} = 0,$$
$$\vdots$$
$$\frac{\partial L}{\partial P_0} = A_c\Lambda_0 + \Lambda_0 A_c^T + \Lambda_1 = 0. \quad (17)$$

Now the problem is to find a matrix K such that (14), (16), and (17) hold simultaneously, which will result in a local minimum for the Lagrangian L in (15).

Optimization Algorithm

In this section, the matrix K is iteratively calculated to satisfy (14), (16), and (17) simultaneously. To this end, the following constrained gradient-based algorithm is proposed:

1) Find an initial matrix K_0 that makes $A + BK_0C$ Hurwitz.
2) At the kth iteration, use K_{k-1} to solve the algebraic Riccati equations (14) and (17) for the matrices P_k and Λ_k, respectively.
3) Substitute K_{k-1}, P_k, and Λ_k in (16) to find $\partial L/\partial K$.
4) Find S_k in terms of $\partial L/\partial K$ as an updating direction for K_{k-1}.
5) Find K_k using $K_k = K_{k-1} + \alpha S_k$, where α is the optimization step size and is chosen such that L in (16) decreases while $A + BK_kC$ remains Hurwitz.
6) Repeat steps 2–5 until $\| \Delta K \|_2 = \| K_k - K_{k-1} \|_2$ becomes smaller than a predefined positive scalar ϵ.

In step 4 of the preceding algorithm, the Broyden–Fletcher–Goldforb–Shanno (BFGS) technique [15], which is a fast descent-direction method of optimization, is chosen to find S_k, which is an updating direction for K_{k-1} in step 5. The BGFS technique is based on a QN method in which the descent direction S_k is

$$\mathcal{V}(S_k) = -H_k\mathcal{V}\left(\frac{\partial L}{\partial K^T}\Big|_{K_{k-1},P_k,\Lambda_k}\right),$$

where the operator $\mathcal{V}(.)$ reshapes an $m \times n$ matrix to an $mn \times 1$ vector by placing all columns of the matrix into a single column and keeping all elements unchanged, and the Hessian matrix H_k is initially set to the identity matrix

$$H_0 = I,$$

and it is iteratively updated as

$$H_{k+1} = H_k + D_k,$$

where D_k is a correction term. In the BFGS technique, the objective is to find D_k to satisfy the following three conditions at each iteration:

1) H_{k+1} is symmetric and a positive definite
2) $\delta K_k = H_{k+1}\delta L_k$ (secant condition)
3) $\delta K_i = H_{i+1}\delta L_i, i = 0, 1, \ldots, k-1$ (hereditary condition),

where δK_k and δL_k are defined as

$$\delta K_k \triangleq \mathcal{V}(K_{k+1}) - \mathcal{V}(K_k)$$
$$\delta L_k \triangleq \mathcal{V}\left(\frac{\partial L}{\partial K^T}\Big|_{K_k,P_{k+1},\Lambda_{k+1}}\right) - \mathcal{V}\left(\frac{\partial L}{\partial K^T}\Big|_{K_{k-1},P_k,\Lambda_k}\right).$$

If $(\delta K_k)^T\delta L_k > 0$, then the preceding three conditions will be satisfied. In the BFGS technique, D_k is defined as

$$D_k = \frac{\tau_k\delta K_k(\delta K_k)^T - \delta K_k(\delta L_k)^T H_k - H_k\delta L_k(\delta K_k)^T}{(\delta K_k)^T\delta L_k},$$

where τ_k is defined as

$$\tau_k = 1 + \frac{(\delta L_k)^T H_k\delta L_k}{(\delta K_k)^T\delta L_k}.$$

Simulations are conducted in the next section to show the effectiveness of the proposed algorithm.

Table 2. The system parameters

Area 1	Area 2	Area 3
$M_1 = 10$	$M_2 = 8$	$M_3 = 8$
$D_1 = .6$	$D_2 = 0.9$	$D_3 = 0.75$
$\tau_{ch1} = 0.5$	$\tau_{ch2} = 0.6$	$\tau_{ch3} = 0.55$
$\tau_{g1} = 0.2$	$\tau_{g2} = 0.3$	$\tau_{g3} = 0.25$
$R_1 = 0.05$	$R_2 = 0.0625$	$R_3 = 0.055$
$T_{12} = T_{13} = 2$	$T_{21} = T_{23} = 2$	$T_{31} = T_{32} = 2$
$B_1 = 20.6$	$B_2 = 16.9$	$B_3 = 18.93$

See Table 1 for an explanation of units.

Simulation Results

A three-area islanded grid presented in Figure 2 with the tie-line interconnection presented in Figure 3 is considered here, and the system parameters are specified in Table 2. To demonstrate the effectiveness of the proposed approach, a decentralized controller is planned that includes three simultaneously designed PI controllers. The parameters of the cost function (12) are chosen as $R = I_{3\times3}$ (3×3 identity matrix), $Q = 10I_{3\times3}$, $V = I_{3\times3}$, $g_{ij} = 10^5$ if $(ij) \in \{13, 14, 15, 16, 21, 22, 25, 26, 31, 32, 33, 34\}$ (otherwise, $g_{ij} = 0$), and $t^k = t^2$. Moreover, $r = [0.2\ 0.2\ 0.2]^T$ is used in this simulation to demonstrate the robustness of the grid to the disturbances.

The history of the optimization cost function J in (12) and the step size α in step 5 of the optimization algorithm in the "Optimization Algorithm" section is demonstrated in Figure 4, which indicates that the optimization algorithm successfully converges, and the cost function is minimized after ten iterations. The history of the six nonzero and 12 zero elements of the feedback gain matrix K in (4) are demonstrated in Figure 5, which indicates that

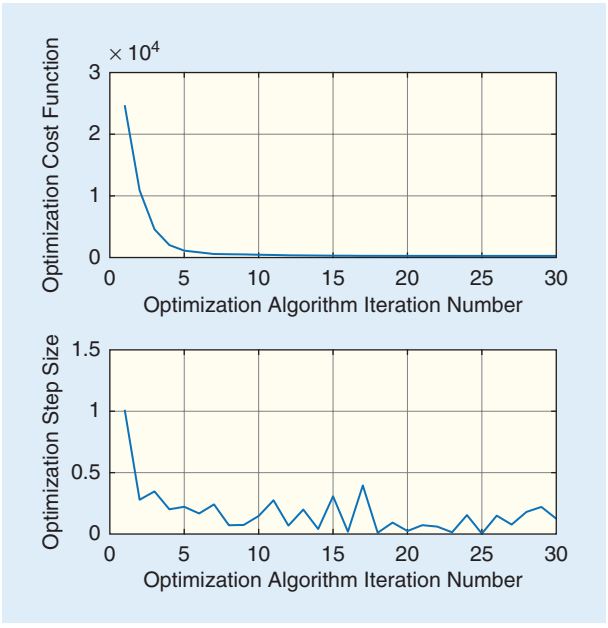

FIGURE 4. The history of the optimization cost function J and step size α.

the decentralized structure is achieved for the feedback gain matrix K.

The six nonzero elements from Figure 5 are augmented to generate the resulting feedback gain matrix

$$K = \begin{bmatrix} -1.38 & 0.13 & 0 & 0 & 0 & 0 \\ 0 & 0 & -1.03 & 0.02 & 0 & 0 \\ 0 & 0 & 0 & 0 & -1.10 & 0.18 \end{bmatrix}.$$

This feedback gain matrix K is used for the realization of the optimal decentralized PI controller in (4). Figure 6 depicts that the ACE, frequency, and tie-line power errors converge to zero, which proves the robust performance of the proposed decentralized controller to the nonzero disturbance $r = [0.2\ 0.2\ 0.2]^T$.

For comparison, the decentralized servomechanism approach [16] is used to design three decentralized optimal LQG-integral controllers for the three areas of the islanded grid. Each eighth-order LQG-integral controller includes a seventh-order LQG controller in series with an integrator to compensate the steady-state error. In the decentralized servomechanism approach, the tie-line interconnections are taken into account to design the decentralized LQG-integral controllers. The three resulting eighth-order LQG-integral controller transfer functions are inserted into the controller blocks i ($i = 1, 2, 3$) in Figure 2 for simulation. The ACE, frequency error, and tie-line power error are depicted in Figure 7. A comparison between Figures 6 and 7 justifies the effectiveness of this analytical work to design the optimal decentralized PI controllers, which have a similar performance but a considerably lower-order structure as compared to the decentralized LQG-integral controllers.

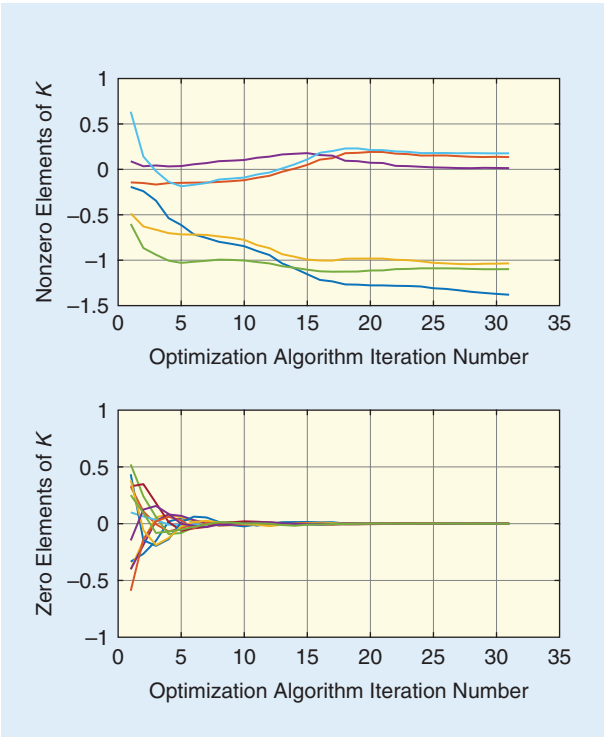

FIGURE 5. The history of the six nonzero and 12 zero elements of the feedback gain matrix K in (4).

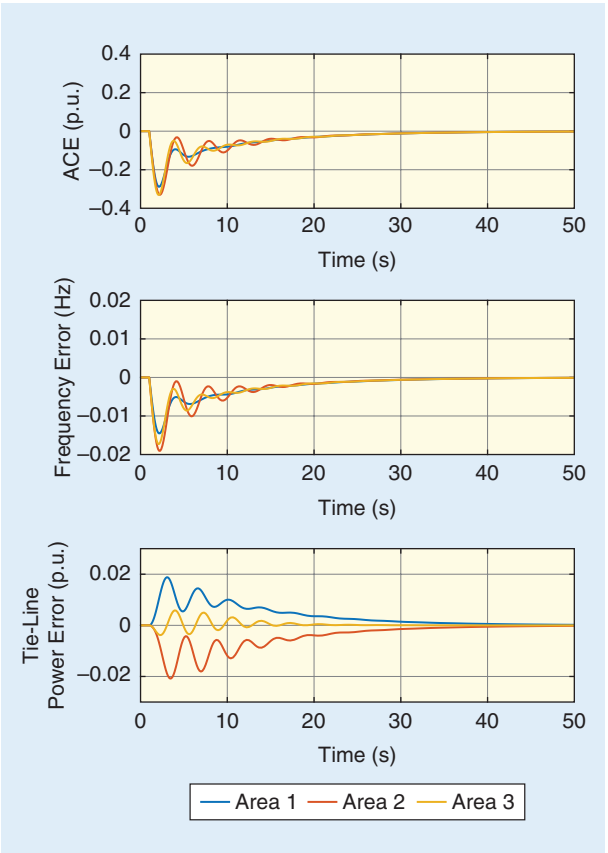

FIGURE 6. The performance of the optimal decentralized PI controller in terms of ACE, frequency error, and tie-line power error.

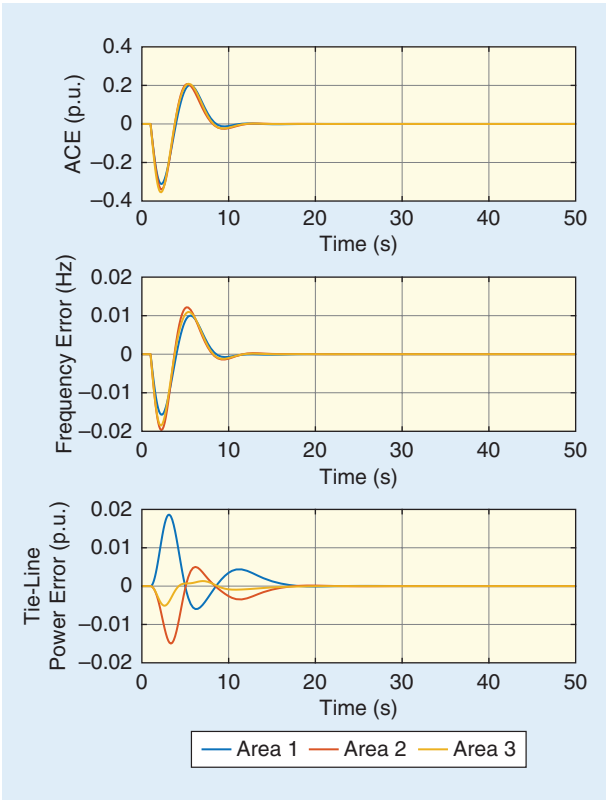

FIGURE 7. The performance of the eighth-order optimal LQG-integral controllers designed in the decentralized servomechanism framework, in terms of ACE, frequency error, and tie-line power error.

Conclusions

In this article, an optimal decentralized PI controller was designed for the LFC of a multiarea islanded grid that included synchronous generators and other distributed generation systems. The proposed decentralized controller had a diagonal structure that was decomposed into a block-diagonal gain matrix and a block-diagonal transfer function matrix. The resulting block-diagonal transfer function matrix of the controller was augmented to the dynamics of the system, while the resulting block-diagonal gain matrix of the controller was used as the design parameter to optimize the cost function. The cost function included two quadratic terms (for input and output energies), a penalty term on the impact of the disturbance, and a penalty term (on the zero elements of the block-diagonal gain matrix of the decentralized controller) that enforced both the optimal and decentralized properties of the controller. The cost function was minimized by means of a descent-direction QN-based optimization method, the BFGS technique.

This optimization technique resulted in an optimal controller with the decentralized PI structure whose performance was robust to the disturbances. Simulation results of a three-area islanded grid justified that the proposed optimal decentralized PI controller, which included three PI controllers designed and optimized simultaneously, had a performance similar to a set of three eighth-order optimal LQG-integral controllers, which were designed in the decentralized servomechanism framework. Moreover, the optimal decentralized PI controllers had a considerably lower-order structure as compared to the LQG-integral controllers.

Author Information

S. Mohsen Azizi (sazizi@mtu.edu) is with Michigan Technological University, Houghton. ***S. Ali Khajehoddin*** is with the University of Alberta, Edmonton, Canada. Azizi and Khajehoddin are Senior Members of the IEEE. This article first appeared as "An Optimization Approach to Design Decentralized Load Frequency Controllers for Synchronous Generators in Islanded Grids" at the 2016 IEEE IAS Annual Meeting. This article was reviewed by the IAS Power Systems Engineering Committee.

References

[1] S. M. Azizi and S. A. Khajehoddin, "Robust load frequency control in islanded microgrid systems using m-synthesis and D-K iteration," in *Proc. 2016 Annu. IEEE Systems Conf. (SysCon)*, pp. 1–8.

[2] Y. Mi, Y. Fu, C. Wang, and P. Wang, "Decentralized sliding mode load frequency control for multi-area power systems," *IEEE Trans. Power Syst.*, vol. 28, no. 4, pp. 4301–4309, Nov. 2013.

[3] H. Bevrani and P. Daneshmand, "Fuzzy logic-based load-frequency control concerning high penetration of wind turbines," *IEEE Syst. J.*, vol. 6, no. 1, pp. 173–180, Mar. 2012.

[4] H. Yousef, K. AL-Kharusi, M. Albadi, and N. Hosseinzadeh, "Load frequency control of a multi-area power system: An adaptive fuzzy logic approach," *IEEE Trans. Power Syst.*, vol. 29, no. 4, pp. 1822–1830, July 2014.

[5] C.-F. Juang and C.-F. Lu, "Load-frequency control by hybrid evolutionary fuzzy PI controller," *Proc. Inst. Elect. Eng.*, vol. 153, no. 2, pp. 196–204, Mar. 2006.

[6] M. Farahani, S. Ganjefar, and M. Alizadeh, "PID controller adjustment using chaotic optimisation algorithm for multi-area load frequency control," *IET Control Theory Applicat.*, vol. 6, no. 13, pp. 1984–1992, Sept. 2012.

[7] H. Chen, R. Ye, X. Wang, and R. Lu, "Cooperative control of power system load and frequency by using differential games," *IEEE Trans. Control Syst. Technol.*, vol. 23, no. 3, pp. 882–897, May 2015.

[8] F. Daneshfar and H. Bevrani, "Load-frequency control: A GA-based multiagent reinforcement learning," *IET Generation, Transmission Distribution*, vol. 4, no. 1, pp. 13–26, Jan. 2010.

[9] S. Saxena and Y. Hote, "Load frequency control in power systems via internal model control scheme and model-order reduction," *IEEE Trans. Power Syst.*, vol. 28, no. 3, pp. 2749–2757, Aug. 2013.

[10] C. Zhao, U. Topcu, and S. Low, "Optimal load control via frequency measurement and neighborhood area communication," *IEEE Trans. Power Syst.*, vol. 28, no. 4, pp. 3576–3587, Nov. 2013.

[11] S. M. Azizi and S. A. Khajehoddin, "An optimization approach to design decentralized load frequency controllers for synchronous generators in islanded grids," in *Proc. IEEE Industry Applications Society (IAS) Annu. Meeting*, Portland, OR, 2016, pp. 1–7.

[12] H. Saadat, *Power Systems Analysis*. New York: McGraw-Hill, 2002.

[13] P. Kundur, N. Balu, and M. Lauby, *Power System Stability and Control*. New York: McGraw-Hill, 1994.

[14] D. Moerder and A. Calise, "Convergence of a numerical algorithm for calculating optimal output feedback gains," *IEEE Trans. Automat. Control*, vol. 30, no. 9, pp. 900–903, Sept. 1985.

[15] R. Fletcher and M. J. D. Powell, "A rapidly convergent descent method for minimization," *Comput. J.*, vol. 6, pp. 163–168, 1963.

[16] E. J. Davison and A. G. Aghdam, *Decentralized Control of Large-Scale Systems*. New York: Springer-Verlag, 2014.